Preliminary 2013 Calibration Report for NISTAR

Steven R. Lorentz, Aaron D. Long, Allan W. Smith

L-1 Standards and Technology, Inc. New Windsor, MD 21776

Contact **Adam Szabo (Project Scientist)**
Adam.Szabo-1@nasa.gov

Contact **Alexander Marshak (Associate Project Scientist)**
Alexander.Marshak@nasa.gov

Contact **Steven Lorentz (NISTAR Instrument Scientist**
Lorentz@l-1.biz

The NIST Advanced Radiometer (NISTAR) is an instrument designed to measure the absolute irradiance reflected and emitted from the sunlit face of Earth as viewed from an orbit around the Earth-Sun L-1 point during the DSCOVR NASA mission. It consists of four detectors: three active cavity radiometers and a photodiode, plus several band-defining optical filters that can be used with any of the detectors. It was calibrated in 2013 against a uniform source similar in setup to that used at the NIST Spectral Irradiance and Radiance Responsivity Calibrations using Uniform Sources (SIRCUS) facility during 2010. The calibration was performed with the NISTAR space-flight instrument in a thermal vacuum chamber in a clean-room environment at L-1 Standards and Technology, Inc. (L-1). This calibration included system-level measurements of the relative spectral response of the NISTAR bands using a wavelength-tunable laser, and absolute responsivity measurements of each of the four NISTAR detectors at 532 nm. This preliminary report includes the results sans the calibrated trap detector response, and the standard uncertainty of these results was 0.16 % (k=1).

Introduction

The NIST Advanced Radiometer (NISTAR) is a NASA spaceflight instrument designed to perform accurate measurements of the total spectrally-integrated reflected and emitted light from the Earth near the L-1 point. It was conceived as an absolute radiometer to fly next to the Enhanced Polychromatic Imaging Camera (EPIC), a NASA multispectral imager, which would be the first ever to view the Earth from this vantage point. Most space-based Earth-observing instruments fly in a low-earth orbit, enabling complete solar-day/night global coverage by scanning a wide enough swath over a twenty-four hour period while the Earth rotates beneath. Others are in a geostationary orbit, where they observe the same large region of the Earth

continuously (though normally scanned), night and day. From an orbit about the L-1 point, which is the neutral gravity point located about 1 % of the distance along the line from the Earth and the sun, EPIC and NISTAR will view essentially the full sunlit Earth disk as the Earth rotates beneath. From this vantage point, the Earth subtends only about 0.5°, which is similar to the angle subtended by the sun or moon as seen from Earth.

The NISTAR instrument was developed from 1998 to 2001 by Ball Aerospace and Technology Corporation, NIST, Scripps Institute of Oceanography, and NASA. During the same period, development of a new detector-based approach to radiometric calibration was being completed at NIST in the Spectral Irradiance and Radiance Responsivity with Uniform Sources (SIRCUS) facility [1]. In this technique, a spectrally tunable laser illuminates an integrating sphere to provide a highly uniform, tunable monochromatic source. This source is then used to calibrate the absolute spectral responsivity of instruments relative to that of a NIST absolute reference detector. An initial attempt to use SIRCUS to calibrate NISTAR was made in 2001, after which some improvements were made to the instrument and the calibration technique. The instrument was calibrated again at SIRCUS in 2003, after which it spent several years in storage at NASA. In 2010, NISTAR was taken out of storage and calibrated using a new portable version of SIRCUS at NIST. In 2013 NISTAR was disassembled at L-1 Standards and Technology, and then reassembled and recalibrated with a SIRCUS-like system. This report describes the results of the 2013 recalibration of NISTAR.

NISTAR Instrument

Fig. 1 shows a solid model of the instrument and a picture of the instrument before installation of its thermal blankets. The instrument consists of the Radiometer Assembly (RA) mounted onto the Interface Control Electronics (ICE) module. The RA contains four optical

radiation detectors: three active cavity radiometers (ACR) and one silicon photodiode (PD), each with its own contamination door, motorized shutter, precision apertures, and baffle. The cross-section of the RA in Fig. 2 shows the photodiode and one of the ACRs. The other two ACRs have an identical design, and are located symmetrically around the center axis of the RA. A twelve-position motorized filter wheel rotates about the center of the RA, and is shown edge-on in Fig. 2. (The contamination doors and shutters do not appear in Fig. 2 simply because it is a cross-section.) All four detector assemblies are mounted onto a common temperature-controlled heat sink (HS) at the base of the RA. The ICE consists of a RAD6000 processor, motor drivers, a MIL-STD-1553 communication interface, and the housekeeping electronics.

The front of each of the four baffle tubes contains a field-of-view (FOV)-limiting aperture, and the rear of each baffle tube contains a primary aperture. Each primary aperture, nominally 8 mm diameter, defines the amount of light from the input irradiance beam that is passed to the PD or ACR immediately behind it. Each FOV-limiting aperture defines a field of view of 1°, and a field of regard (FOR) of 7°, for its respective detector. The FOV is the full angular range over which a collimated incident beam is not vignetted. The FOR is the angular range beyond which no light from a collimated source reaches the detectors directly.

Each ACR consists of a black-painted conical metal receiver cavity (RC) mechanically linked to the HS through a carefully-designed Kapton tube. Each RC also contains a 4-wire resistive wire-wound heater and a 4-wire positive-temperature-coefficient (PTC) thermistor. These are affixed to the rear surface of each RC using Stycast epoxy. To minimize the radiative coupling of the RC with its surroundings behind it, the rear surface of each RC was coated with gold. The leads to the RC heater and thermistor were designed with materials and dimensions so as to minimize their contribution to the thermal conductive coupling between the RC and the HS.

The Kapton tube is the mechanical link between the RC and the HS. It was designed as the primary thermal link between the RC and the HS, meaning that heat conduction through the Kapton tube is much larger than the heat conduction along any electrical wires between the RC and the HS, as well as the radiative coupling from the RC to the HS. Any optical or electrical radiation that is absorbed within the RC heats it slightly relative to the HS, and the locations of the heater and thermistor were chosen so as to minimize the non-equivalence between optical and electrical heating of the RC. The HS has a wire-wound heater rand a PTC thermistor. The electronics in the ICE provides independent digital servo loops that control the temperature (as monitored by the resistance of each PTC) for each RC and the HS, by controlling each heater to a programmable value for the respective PTC thermistor. When the shutter opens, the change in required electrical power is accurately measured by A/D converters in the ICE, and this change in electrical power provides a measure of the change in total spectrally-integrated optical power that enters the RC. The electrical power change is nearly equal to the optical power change to within a few percent for such ACRs, so the calibration is nearly predictable. However, the requirements for NISTAR irradiance scale accuracy are well below 1%, so to meet them the ACRs were specifically calibrated as described in the sections to follow.

The PD generates a current proportional to the irradiance reaching it, and this is monitored by the ICE. Measurement of the relationship between that current, as read out by the ICE, and the input irradiance (over a limited wavelength range) was also part of the NISTAR calibration, and this is included in the results below.

NISTAR has three wide spectral bands, denoted A, B, and C, as represented in Fig. 3. Band A is simply a totally unfiltered RC, enabling a measure of the solar reflected and Earth emitted irradiance. Bands B and C are defined by filters. Band B covers the solar-reflected

irradiance, and Band C covers only the near-infrared part of the solar-reflected irradiance. The filters are distributed on the twelve-position filter wheel as shown in Fig. 4. Of the twelve filter positions, only six are populated with filters: three Band B and three Band C. The remaining six filter wheel positions are left open, all therefore defining Band A. The detectors, labeled RC1, RC2, RC3, and SP (silicon photodiode) in Fig. 4, are each located behind filter position 1, 4, 7, and 10, respectively, when the filter wheel is in the normal position depicted here. Note that this enables each of the RC's to measure a different band; in this case RC1 is band C, RC2 is Band A, and RC3 is Band B. The motorized filter wheel can be rotated about its center axis so as to position different combinations of filters in front of the four detectors. Note, in particular, that any filter can be positioned in front of the silicon photodiode, a feature that enables in-situ measurements of the transmittance of the filters during calibration as will be described below.

Note that for any populated Band B or Band C filter position, the band-pass filter is followed by a separate thermal blocking filter, as shown in the cross section of the filter wheel in Fig. 2. The thermal-blocking filter substrate is made from the same material (fused silica) as the band-pass filter substrate, but is mechanically and thermally separated so as to present a more thermally stable scene to the ACR. Note that there is no thermal blocking filter in the Band A filter positions, just a hole. For all twelve positions of the filter wheel, these holes are large enough that they do not vignette the incident beam defined by the FOV-limiting and primary apertures discussed above.

System-Level Calibration

Configuration

The NISTAR instrument was located in the NISTAR vacuum chamber as shown in Fig. 5. This vacuum chamber enables the instrument to be held at its operating temperature, in a vacuum, while surrounded by a black shroud maintained at the temperature of liquid-nitrogen, in order to simulate space-like thermal conditions. The front flange of the chamber includes four ports, each of which is co-aligned with one of the four optical axes corresponding to the NISTAR instrument detectors (the three receiver cavities: RC1, RC2, RC3, and the silicon photodiode: PD). Each of these ports has an individually-removable optical window. Only two of these NISTAR ports and chamber windows appear in the cross-section of Fig. 5; the other two are out of the page along the y axis. The NISTAR chamber windows are each made from UV-grade fused silica, 1.5 inch diameter, 0.25 inch thick, antireflection-coated on both sides for the spectral range 425 nm to 675 nm, and they have a wedge angle less than 5 arc-minutes.

An L-1 Standards and Technology photodiode trap detector was used as the reference detector. This trap detector, LTD-11, Serial Number (SN) 109 (henceforth referred to as T-109), was mounted on the side of the NISTAR chamber as shown in Fig. 5 with its optical axis parallel to the four optical axes of the NISTAR instrument, along the z axis. A trap detector is composed of several (typically three or more) silicon photodiodes arranged optically in series such that the reflected light from the surface of the first photodiode is incident on the second photodiode, the reflected light from the surface of the second photodiode is incident on the third photodiode, etc. The photocurrents from all of the individual photodiodes are added at the input to the trans-impedance pre-amplifier, which converts the total photocurrent to a voltage signal. The type of large-area silicon photodiodes used have internal quantum efficiency of near 100 % at visible to

near-infrared wavelengths, so in the trap arrangement a well-designed and maintained trap detector has nearly 100 % external quantum efficiency.

The trap detector used here, T-109, had a circular precision knife-edge aperture, with a nominal diameter of 5mm. When this black aperture is illuminated with a collimated beam that overfills it, the well-defined beam that passes through it enters the trap detector. This trap detector therefore enables measurement of the irradiance of the incident beam, as will be described later. The trap detector was mounted such that the plane of its aperture was located in the same plane as that of the four NISTAR detector primary apertures, to within 1 mm (Fig. 5). A picture of the chamber in the clean room is shown in Fig. 6a.

The light sources consisted of a frequency-doubled Nd:Vanadate laser at wavelength of 532 nm and a wavelength-tunable Ti:Sapphire laser located on an optical table inside of the clean room, shown in Fig. 6b. After passing through a variable attenuator that enabled intensity stabilization, the beam was focused into a multi-mode silica fiber-optic cable. Prior to the fiber input, a small fraction of the beam was diverted to a wavelength meter. An un-sheathed section of the fiber-optic cable was passed through an ultrasonic water bath, which served to smooth out laser speckle.

The fiber output end was connected to a Spectralon integrating sphere shown in Fig. 5. A precision aperture at the output of this sphere was located at the focus of a two lens system, which served as a collimator for the laser light that exited the sphere. Also, a shutter was located after the aperture to enable blocking the laser beam from entering NISTAR for background measurement. The entire sphere/collimator assembly was mounted on an x-y translation stage, which enabled the collimated beam to be directed along any one of the four NISTAR detector optical axes, or along the axis of the trap detector. The precision aperture diameter and

collimator effective focal length were chosen to provide a 0.6° angular divergence, to simulate that of the Earth as viewed from an L-1 orbit. The nominal beam diameter was 20 mm, sufficient to overfill the front aperture of any one of the NISTAR detectors (and the trap detector aperture), but it was not large enough to stimulate more than one detector at the same time. Black baffles were positioned at various locations, including one around the beam (indicated in Fig. 5), to reject stray light.

A silicon photodiode was mounted on a third port on the top of the integrating sphere and monitored the laser intensity inside of the sphere. Its photocurrent was passed through a dedicated trans-impedance pre-amplifier, whose output voltage signal was used as the feedback for the laser intensity stabilization servo system. It was also recorded in the data files and was stable for each measurement to about 10ppm.

In order to minimize the background light, the clean room lights and the regular room lights were turned off during the measurements. A small but noticeable amount of stray light was present, primarily from the laser, and the photodiodes also registered a small DC background response even when no light is applied, as is normal. Therefore a background measurement was performed for the photodiode and trap detectors. This consisted of simply measuring the silicon photodiode response and the trap detector response with the laser on and the integrating sphere shutter in its off state.

The NISTAR instrument was operated using its standard set of ground-support equipment (GSE). The two racks that support this equipment, as well as the support computers, were located right outside of the clean room. A LabVIEW program running on the standard NISTAR GSE computer provided the operator interface to the NISTAR instrument, and performed automated data acquisition. Other equipment unique to this test setup, such as the

laser wavelength meter, the external laser shutter, the translation stage, the voltmeter for the trap photodiode response, and the voltmeter for the monitor photodiode response, were interfaced to this computer and the LabVIEW software was configured to incorporate them as necessary.

Assessment of the collimated beam irradiance uniformity and alignment in the x-y plane relative to NISTAR and the trap detector was performed by scanning the beam across these detectors. Figure 7 provides the results from scanning the collimated light beam across both the trap detector and the NISTAR photodiode, stopping at each position while recording the respective detector voltage signal. When making these scans, the detector signal (either the trap or the PD) was recorded at each position along the scan axis, and these were normalized to the value at the radiometric center of the beam. Prior to measuring these data, a series of similar scans, alternating first along the x axis and then along the y axis, were made and used to find the stage x and y coordinates corresponding to the radiometric center for these two detectors. The stage coordinates of the center positions of the three NISTAR ACRs would have been much harder to determine radiometrically because of the longer time constants of the ACRs. However, the x and y positions of the ACR optical axes are known relative to the PD from the mechanical design, so the stage coordinates of the ACRs were known once the radiometric center of the PD was found.

Method for System-Level Relative Spectral Calibration

The relative spectral calibration of NISTAR is based on measurements of the filter transmittance of each of the six filters (three Band B; three Band C) at each wavelength across the spectral range. Because the wavelength spectrum of interest for NISTAR is extremely broad, covering the ultraviolet through the infrared, it would be necessary to combine a variety of instruments and techniques to achieve high spectral resolution while maintaining high accuracy.

In 2010, there were two complementary techniques used: *piece-parts* and *system-level*. In the piece-parts technique, the transmittance of each of the six filters was measured separately in standard NIST transmittance facilities prior to installation in the NISTAR instrument. For wavelengths below 1600 nm, this was done using a NIST grating-monochromator-based facility. For wavelengths above 1000 nm, this was done using a NIST Fourier-Transform Spectrometer (FTS)-based facility. In the system-level technique, the transmittance measurements were made with the filters installed in the fully-assembled instrument, in the chamber, in a configuration similar to the one described in the previous section (Fig. 5). For 2013, only the system-level measurements were performed, and these were used to scale the 2010 calibration. Any change in the transmittance of the filters from cleaning was assumed to be spectrally flat.

While a piece-parts technique has the advantage of complete spectral coverage, its disadvantages are that system-level inter-reflections, stray light, and beam geometry are not directly measured. In contrast, the system-level technique includes these effects in its measurement results. Another advantage, is that it can be performed without requiring disassembly of the instrument, which is a particularly important concern for the NISTAR instrument or any other space-flight instrument where a re-calibration is desired closer to its launch date. A disadvantage of the system-level calibration is that automated, tunable lasers, are not available to cover the entire spectral range of interest, which covers the UV to the far-IR. Therefore, the approach used here was to perform the system-level measurements in the critical spectral regions where they are most useful, and to use these data as tie-points to correct the full-spectral range, piece-parts filter transmittance data.

The 2013 relative spectral calibration of the NISTAR instrument consisted of performing a system-level measurement of the transmittance of each of the six NISTAR filters in the 700 nm

to 750 nm range. The light source for these measurements was the tunable Ti:Sapphire laser, integrating sphere, and collimator assembly as described above. The NISTAR PD was used as the detector, and the x-y translation stage was positioned to illuminate the PD through the corresponding NISTAR PD chamber window. Transmittance measurements require both a set of "filter-in" PD response measurements, with the given filter in the beam, and a set of "filter-out" PD response measurements, with the filter out of the beam but all else unchanged. The ratio of background-subtracted filter-in response to background-subtracted filter-out response then gives transmittance, as discussed in the analysis section below. To perform each filter-in measurement set, first the NISTAR instrument was commanded, though its normal test-mode telemetry, to rotate the filter wheel so as to position that filter in front of the PD. Then the PD response, the monitor photodiode response, and the wavelength meter reading were recorded as the Ti-sapphire laser was tuned through its wavelength range while the filter wheel remained at that position. The process for performing each filter-out measurement set was similar, except that the filter wheel was rotated to a position where there was no filter in front of the silicon photodiode. A single filter-out measurement was measured prior to the measurement of each filter set. Each filter-out measurement set was performed at the same set of wavelengths as its corresponding filter-in measurement set to within 0.1 nm, but it was in general not possible to tune to precisely the same wavelengths in each set. The timeline during which the filter measurements were performed is given in Table 1, and the other data such as file names for each set is given in Table 2a.

The procedure of measuring each entire filter-in spectrum separately from its corresponding filter-out spectrum was chosen over the alternative, performing a single filter-in and filter-out measurement at each wavelength, since the latter would have required moving the

NISTAR filter wheel twice for each wavelength point. This would have been time-consuming and caused unnecessary wear to the filter wheel mechanism. The procedure used was enabled by the remarkable intensity stability of the tunable laser.

Method for Absolute Calibration of Active Cavity Radiometers

The system-level absolute irradiance responsivity of each of the four NISTAR detectors was measured at 532 nm using the setup described in the configuration section above. Responsivity measurements involve a ratio of detector response to input irradiance, and these two quantities were measured separately from each other. The response and general character of the three NISTAR ACR receiver cavities (RC), being thermal detectors, is quite different than that of photodiodes: each RC response measurements required a long train of regularly shuttered measurement cycles, each 10 minutes long, whereas irradiance measurements using the trap detector required only one relatively short shutter cycle. For each response measurement, the stage was first positioned to align the collimated laser beam at 532 nm with the corresponding NISTAR detector. The NISTAR internal shutter for that NISTAR detector was left in the open position, and the NISTAR filter wheel was rotated to the position whereby there was no filter in front of any of the NISTAR detectors (Band A, Fig. 4). The NISTAR heat sink servo was set to control the heat sink at a constant PTC thermistor value of 7500 ohms, corresponding to slightly above ambient temperature. The NISTAR instrument was operated in vacuum and at its operating temperature, and the NISTAR chamber shroud was maintained at liquid nitrogen temperature. Also, the window ports of the NISTAR chamber were placed under temperature control using a dedicated system to minimize drift of the thermal infrared background emitted by the windows.

For each response measurement of a given RC, the servo for that RC was set to control the PTC thermistor for that RC to a constant temperature, corresponding to an applied heater power of approximately 25-50 μW, depending on the run. This provided headroom in anticipation of a shuttered optical power of roughly 1.5 μW, along with plenty of margin to accommodate thermal infrared background drifts. Servos for the other RC's were typically open for the other RC. All servos were allowed to settle before starting shutter cycles. The feed-forward algorithm was also used for the active RC, and allowed to settle prior to starting shutter cycles.

Shutter cycles were performed using the external shutter that modulated the 532 nm laser beam output from the integrating sphere. The cycles were 10 minutes long, consisting of 5 min. with the shutter open, followed by 5 min. with it closed. The NISTAR data-logging PC recorded N = 600 samples per shutter cycle, each equally spaced in time. Each sample consisted of simultaneous measurements of all available quantities, such as RC heater power measured, monitor response, etc. These measurements were automatically written by the NISTAR LabVIEW-based data-acquisition program to tab-delimited spreadsheet files having a pre-defined format, one for each run, for post-acquisition processing. In any given run there were at least 44 shutter cycles of stabilized data, corresponding to more than 7 hours of data collection, with many of the runs having over 90 cycles and over 15 hours of data collection. As shown in the timeline (Table 1), such shutter cycle response-measurement runs were performed three times for RC2 and twice for RC1 and RC3.

Note that all NISTAR internal shutters were left open at all times during the 2013 calibration measurements. Some measurements had been made using internal shutter cycles during the 2003 calibration, but this was not the case during the 2013 calibration. Using the

external shutter more effectively rejects the laboratory environment and chamber window light in Band A, neither of which will be there on flight. However, the internal shuttering, which will actually be used in flight, does result in a thermal perturbation when it is cycled and that will not be captured here. But, it was felt that enough information about internal shuttered cycles was collected in 2003, and the key objective of the 2013 calibration was to update the responsivity calibration.

The trap photodiode response and the NISTAR photodiode response at 532 nm were recorded immediately before or following each RC shutter cycle run (Table 1). These consisted of smaller runs, typically about two minutes long, with the external shutter open. For each run, the collimator was first aligned with the appropriate detector, the trap photodiode or the NISTAR photodiode, prior to the run. The monitor photodiode response was recorded simultaneously to monitor the stability of the laser. The trap photodiode response was used, after application of corrections as discussed in the analysis section below, as the measurement of the shuttered 532 nm irradiance incident on the NISTAR detectors during calibration. These irradiance values will be reported in the full calibration report once the trap has been calibrated at NIST, however they were on the order of 3 $\mu W/cm^2$. This irradiance was found to give an adequate signal to noise ratio for the measurement times used in this calibration, and the discrepancy between this irradiance value and the values used in past calibrations is believed to have a negligible effect due to the linear response of the instrument. For comparison, the on-orbit full-disk Earth irradiance signal measured by NISTAR Band A is expected to be of order 1 $\mu W/cm^2$.

After the absolute response measurements with the chamber under vacuum, the transmittance of each of the four NISTAR chamber windows at a wavelength of 532 nm was measured (Table 1). This was performed as a system-level measurement using the same

configuration described above, except that the chamber was purged with dry nitrogen at atmospheric pressure. Only the NISTAR photodiode was used. The collimator was aligned with the NISTAR photodiode port, and transmittance measurements were made for each of the four chamber windows using the following procedure. The 532 nm laser was stabilized, and a regular sequence of NISTAR photodiode samples was recorded. Initially, no window was on the chamber photodiode window port, so the photodiode measured the "window-out" data. Then, the window under test was installed in the chamber window mount and the photodiode "window-in" data was measured. The process was performed on all four windows, but always using the NISTAR photodiode port, since the RC's do not provide adequate measurements under ambient atmospheric conditions. Each window was rotated inside the mount accordingly to account for the angular offset between the various RC window mounts and the PD window mount. The data were saved as tab-delimited text files for the analysis described below.

Method for Spectral Responsivity Calibration of NISTAR Photodiode

After measuring the filter transmittance, but prior to window transmission measurements and venting the NISTAR chamber, on October 22, 2013 the spectral irradiance responsivity of the NISTAR PD was measured over the spectral range 700 nm to 750 nm. This was done by tuning the Ti:Sapphire laser across this segment of the spectral range, and recording PD and trap detector spectral responses. The filter wheel was in a Band A (no filter) position, and the PD shutter was open. For a given segment, the beam was aligned with the NISTAR PD during the entire segment spectral scan and the PD response, the monitor photodiode response, and the wavelength meter reading were recorded as the Ti-sapphire laser was tuned through the segment spectral range. Then the beam was moved via the x-y stage to align it to the irradiance trap detector, and the trap detector response, monitor photodiode response, and the wavelength were

recorded as the Ti-sapphire laser was tuned through the segment spectral range. Each trap spectral response scan segment was performed at approximately the same set of wavelengths as its corresponding PD response scan segment, but it was in general not possible to tune to precisely to the same wavelengths between the two scans. The file name for each PD and trap detector segment is given in Table 2b. A trap detector segment scan was measured corresponding to each PD segment scan, though sometimes it preceded the corresponding PD segment scan and sometimes it followed.

Analysis and Results

The full radiometric calibration of NISTAR consists of the determination of the absolute irradiance responsivity versus wavelength for the entire spectral range and for each NISTAR detector/filter combination. For an instrument such as NISTAR, this separates into two tasks. One task is the determination of the relative spectral responsivity as function of wavelength, and is described in the Relative Spectral Calibration section below. The other task is the determination of the absolute responsivity at one particular wavelength, and is described in the Absolute Calibration section below. The 2013 calibration performed by L-1, in conjunction with the 2010 SIRCUS calibration, provides key information for both tasks that together enable the calibration of NISTAR.

Relative Spectral Calibration

The black-painted NISTAR receiver cavities are assumed to have negligible variation of absorptance over the spectral range. This is justified based upon NIST experience with reflectance measurements of flat samples of the specular black paint used (Z302) over the entire spectral range of interest, coupled with experimental verification of the cavity enhancement of

the Z302 black-paint absorptance of the actual NISTAR flight receiver cavities through visible-band laser measurements of the total-integrated cavity reflectance. From the results of these measurements, made in 2003 just prior to installation of the flight RC's into the NISTAR instrument as part of the 2003 instrument refurbishment, the reflectance of each cavity is verified to be about 2×10^{-4} (Fig. 8). As the cavities are opaque, the absorptance is given by one minus the reflectance, so the spectral variation of the total-integrated reflectance typically expected in Z302 black-painted cavities becomes negligible (< 0.05 %). Thus to within the 0.1 % (k = 1) level of uncertainty required, the relative spectral response function of the three NISTAR RC's for Band A (no filter) is taken to be flat across the spectral range, and that for Band B and Band C is determined entirely by the relative spectral transmittance of the respective filters.

The piece-parts transmittance measurements of all three NISTAR Band B filters as measured before installation into the NISTAR instrument are plotted in Fig. 9, and those for the NISTAR Band C filters are plotted in Fig. 11. These measurements were made prior to 2010, and they were always made as interference filter paired with thermal-infrared blocking filter, in a specially-designed holder to space them at the same distance as in the actual flight filter wheel (Fig. 2). Also shown in both of these figures are results of 2010 SIRCUS system-level transmittance measurements. For the purposes of this report, these data are presented as background information. The three Band B filters have the spectral limits expected for the high quality water-free quartz material that was used. The three Band C filters show the desired cut-on transition at 720 nm to 730 nm provided by the interference coatings, and the cut-off in the infrared from the high quality water-free quartz substrates. Above the transition, the spectral transmittance of the Band C filters exhibits ripples from the interference coatings. The 2010 SIRCUS system-level transmittance provides confirmation of this behavior, though the values

are slightly higher in general. The purpose of the 2013 system-level transmittance measurements was to improve and update these 2010 SIRCUS system-level measurements.

The results of the 2013 system-level transmittance measurements are plotted in Fig. 10 for Band B and Fig. 12 for Band C. Although the resolution is lower than that of the 2010 measurements and the spectral range is narrower, the results still serve to tie in the old data to the new.

The values of transmittance plotted in Fig. 10 and Fig. 12 were obtained, for each filter, by dividing the background removed filter-in response spectrum by the corresponding background removed filter-out response spectrum as identified in Table 2a. Since the wavelength setting on the Ti:Sapphire was driven by a stepper motor controlled through LabView, each set of raw spectra was paired based upon the position of the stepper motor, as determined by a single transition point and a time series analysis. Each pair of raw wavelengths was determined to be repeatable to within a 0.1 nm of each other and since the response of the photodiode in the linear region is proportional to wavelength, it was determined that a method using interpolations was not needed as this approximation only adds approximately 0.01 % to the uncertainty.

The wavelength scale for the 2013 system-level measurements was that of the wavelength meter used to measure the tunable Ti:Sapphire laser. This wavelength meter is based upon a Michelson interferometer with a stabilized HeNe laser reference (Burleigh Model WA-20DL). The uncertainty in wavelength is less than 0.001 nm ($k = 1$).

These results were fit to the 2010 system level measurements and the correction factor uncertainty was approximately 0.1 % ($k=1$). The scaled 2010 values are also plotted in Fig. 10 and Fig. 12. Table 2b contains the correction coefficients determined for each filter.

Absolute Calibration

A typical example of an absolute NISTAR receiver cavity response (in this case RC2) to the periodically shutter cycled 532 nm irradiance beam is shown in Fig. 13. In Fig. 13a, the full set of raw data for both the NISTAR RC2 measured heater power and the integrating sphere monitor photodiode are plotted versus measurement time. A subset of that data is plotted on an expanded time scale in Fig. 13b. The difference between the RC heater power measured with the shutter closed and that measured with the shutter open is very nearly the optical power measured by that RC through its fully-illuminated 0.5 cm^2 (nominal area) aperture, except for several corrections to be described below.

First, the difference in RC heater power was computed in a way that minimizes the effect of the drift seen in Fig. 13a and the noise seen in Fig. 13b, using the NISTAR post-processing demodulation algorithm. This is a phase-sensitive detection algorithm described by

$$r_J = real\left[\frac{\sum_{M=J-N+1}^{J}\sum_{L=M}^{M+N-1}\sum_{K=L-N+1}^{L}\sum_{I=K}^{K+N-1} e^{i2\pi I/N}\phi_I}{\sum_{M=J-N+1}^{J}\sum_{L=M}^{M+N-1}\sum_{K=L-N+1}^{L}\sum_{I=K}^{K+N-1} e^{i2\pi I/N}\psi_I}\right] \quad (1)$$

where Φ_I is a sequence of raw RC heater power samples, Ψ_I is a corresponding sequence of shutter position values where 0 indicates shutter closed and 1 indicates shutter open, N is the number of samples per shutter cycle, and r_J is sequence of processed RC response measurements. This demodulation algorithm was implemented on an analysis PC using Octave. The values of Φ_I and Ψ_I were input as time-ordered arrays having index I, directly from the raw data spreadsheet file, and the values of r_J were output as a time-ordered array having index J, directly to a processed spreadsheet file. The shutter values were from the shutter data column.

Eq. (1) implements a four-boxcar phase-sensitive detection that performs the required subtraction of the shutter-closed and shutter-open RC heater power values in the frequency domain, effectively rejecting any signals not at the shutter frequency. As an example of the results from this step in the analysis, the demodulated RC2 heater power shutter cycle train of Fig. 13 is plotted in Fig. 14. Fig. 14a plots the input values of Φ_I versus time, and Fig. 14b plots the output values of r_J versus time. The mean value of r_J was used as the RC response r'_N for the shutter cycle set, and the standard deviation of r_J divided by the square root of the number of independent measurements was used as the uncertainty dr'_N of the RC response for that set. For the four-boxcar filter of Eq. (1), the time window for independent measurements is 4 shutter cycles, which is 40 minutes. Thus there were about 20 independent measurements made for a typical 15-hour shutter cycle data set. In the subscripts above, the "N" stands for "NISTAR", and the prime indicates that the power scale used is that of the NISTAR electronics before applying any explicit power scale calibration correction. This uncorrected NISTAR response was computed for all 7 shutter cycle data sets measured during the 2013 calibration, and the results are in Table 3.

The monitor photodiode in the integrating sphere was recorded during each run and determined to be flat on the order of 10ppm throughout each run. As this variation was well below the measurement capabilities of the RCs, it was determined that there was no gain from normalizing the RC value to the value of the monitor PD.

Next, a measurement equation was used to collect all the terms required to calibrate the uncorrected NISTAR response relative to the NIST scale and thereby compute the calibrated NISTAR irradiance responsivity R_N for each RC. The measurement equation applied to each NISTAR RC is

$$R_N = \left[\frac{G_T R_T}{B\tau_w r_T}\right]\left[\frac{r'_N}{A_N}\right] \quad (2)$$

Here the first bracket provides the transfer of the source scale to NISTAR, through the measured trap photodiode response $r_{T,}$ the trap irradiance responsivity R_T, the trap pre-amplifier gain G_T, and the NISTAR chamber window transmittance τ_w for that particular RC. The beam irradiance non-uniformity correction factor B is also included, and will be described below. The second bracket simply computes the NISTAR irradiance measured vs using its native, uncalibrated scale where A_N is the aperture area for that particular RC. In other words, the first bracket of Eq. (2) is the inverse of the actual irradiance level used to calibrate NISTAR, and R_N is expected to be near one based on piece parts characterizations of the NISTAR cavities.

For each trap response data set shown in Table 3, the r_T was computed by calculating the mean of the trap response data set then subtracting the trap background. The standard deviation dr_T was computed as the relative standard deviation of the trap data.

For each NISTAR chamber window, the window transmittance at 532 nm, τ_w, was computed by dividing the mean of the window-in response measurements by the mean of the window-out response measurements. The standard deviation, $d\tau_w$ was also computed for each window as the standard deviation of the window-in measurement added in quadrature with the standard deviation of the window-out measurements. The results are shown in Table 4.

To assess the slight non-uniformity of the irradiance of the beam used to perform the calibration, the beam was scanned perpendicularly across the trap detector in x (horizontally) and y (vertically) (See Fig. 5 for x-axis and y-axis definitions). Figure 7 plots the results of these scans, along with similar scans across the NISTAR photodiode. The NISTAR detector apertures have a nominal diameter 8 mm, while the trap detector irradiance standard aperture had a nominal diameter of 5 mm. To correct for the beam spatially-integrated irradiance mismatch

due to this difference of aperture diameters, the mismatch factor B was computed as the average of trap irradiance values (relative to the trap at center position) within the aperture of NISTAR. The uncertainty of B, dB, was computed as the standard deviation of these relative irradiance values, and its value is included in Table 5.

The trap photodiode irradiance responsivity R_T value will be determined by calibrating the power responsivity of the L-1 trap detector traceable to a cryogenic electrical substitution radiometer at NIST. The aperture area will also be traceable to NIST facilities. These measurements will occur prior to the submission of the full calibration report and the numbers will be included in that report. Because of the high spatial uniformity of this trap detector, the irradiance responsivity will simply be the power responsivity times the aperture area, giving the value of R_T. During the 2013 NISTAR calibration, this trap was used with a pre-amplifier. The gain of this pre-amplifier is nominally 10^7 V/A and it will also be measured prior to the submission of the full report. The NISTAR aperture area A_N values used are from measurements made on each NISTAR aperture before NISTAR was assembled, prior to 2001 at the NIST aperture area measurement facility [2]. This is the same facility that will be used to measure the trap detector aperture area. Taking the ratio of the cavity response to the area computes the irradiance response of the NISTAR cavity in W/cm^2. The watts expressed here are watts as output by the NISTAR electronics and do not necessarily represent a watt as is meant in the first bracket of Eq. (2). The final units then, are in W_N/W, where W_N indicates uncorrected watts as output from the instrument. The value of this ratio is expected to be close to unity because that is how the instrument was designed (i.e. it was built to output a 'watt' with a value close to a real watt). Any deviation from unity represents the inability to construct a perfect instrument and this ratio is the calibration factor sought in this report. That is to say, we want to know how many

watts NISTAR says is incident on the cavity for every 'real' watt that is incident on the cavity. Restated, Eq. (2) appears thusly,

$$R_N = [G_T R_T] C_N \tag{3}$$

Here, C_N represents an uncalibrated NISTAR irradiance responsivity coefficient. A summary of the parameters of Eq. (2) is given in Table 5. The uncalibrated irradiance responsivity C_N (Eq. 3) was computed separately for each shutter cycle data set for each RC, and these are reported as separate rows in Table 5. The combined standard uncertainty dC_N listed in Table 5 was computed for each shutter cycle data set for each RC as the quadrature sum of the relative uncertainties of each of the components of Eq. (2). A plot of these results for each RC is shown in Fig. 15. Without the calibrated values of the trap detector response and the gain of the trap pre-amplifier, the value of the NISTAR cavity irradiance responsivity cannot be reported in this preliminary report and must be reported as a cavity specific scale factor in units of W/(Vmm^2) with the remaining factors left as constants. However, these unknown factors are independent of the NISTAR cavity being measured and independent of the particular measurement, so the known factors still indicate cavity and inter-cavity repeatability. The uncertainty of this correction factor less the trap calibration was of order 0.1 % (k=1) and the largest contributor to that can be seen from Table 5 to be the cavity measurement itself.

PD Spectral Irradiance Responsivity Calibration

The results of the 2013 system-level NISTAR PD irradiance responsivity calibration analysis are plotted in Fig. 16. These results were obtained by dividing the PD response spectrum by the corresponding trap detector response spectrum for the range of 700 nm to 750 nm, as identified in Table 2c. As with the filter measurements, the raw spectra pairs were determined

by a time series analysis implemented in Octave. The mean of each group of background subtracted PD values were ratioed to the mean of the corresponding background subtracted trap values. The 0.1 nm uncertainty in the wavelength results in less than 0.01 % additional uncertainty as described in the filter measurements section, above. In order to fit the 2010 data to the 2013 data and find the corrected spectral irradiance responsivity of the PD, these ratios must be multiplied by the calibrated spectral response of the trap detector which, as with the previous sections, will be supplied in the full calibration report. The resulting values will then be fit to the 2010 measurements, which were of much broader range and more highly sampled spectrally. This correction factor obtained from this fit is anticipated to have an uncertainty of less than 0.1 %. The results for the 2010 PD responsivity and PD to trap ratios are plotted in Fig. 16.

Summary

This preliminary report describing the 2013 calibration of NISTAR reports the change in filter transmission relative to the 2010 measurements (Table 2b) as well as the repeatability and relative inter-cavity response of the NISTAR receiver cavities (Table 5). The full report will include a full discussion of these findings as well as the absolute calibration figures for the NISTAR cavities and the responsivity of the NISTAR photodiode. These measurements are subject to the determination of the calibrated spectral responsivity of the L-1 trap detector used in this report.

References

1. S. W. Brown, G. P. Eppeldauer, and K. R. Lykke, "Facility for spectral irradiance and radiance responsivity calibrations using uniform sources (SIRCUS)," *Appl. Opt.* **45**, 8218 (2006).
2. J. Fowler and M. Litorja, "Geometric area measurements of circular apertures for radiometry at NIST," *Metrologia* **40**, S9-S12 (2003).

Table 1. Timeline of 2013 NISTAR calibration-related activities. The first column refers to the date in 2013 during which the activity took place. The "Notebook Page" here in the second column and in the other tables refers to the page numbers in the "NISTAR 2010 & 2013" laboratory notebook recorded by S. R. Lorentz.

Date	Notebook Page	Activity
8-Aug	65	Chamber setup
25-Sep	69	Install trap next to NISTAR chamber in same plane as aperture
1-Oct	70	Mapped center of PD and Trap
9-Oct	76	Measure beam uniformity with trap
9-Oct	76	Measure RC1 response
10-Oct	76	Measure beam uniformity with trap and PD Response
10-Oct	76	Measure RC2 response
10-Oct	76	Measure PD response
10-Oct	77	Measure beam uniformity with trap and adjusted optics
10-Oct	77	Measure beam uniformity with trap and PD response
10-Oct	77	Measure RC3 response
11-Oct	77	Measure beam uniformity with trap and PD response
11-Oct	77	Measure RC1 response
12-Oct	78	Measure beam uniformity with trap and PD response
12-Oct	78	Measure RC2 response
13-Oct	78	Measure beam uniformity with trap and PD response
13-Oct	79	Measure RC3 response
14-Oct	79	Measure beam uniformity with trap and PD response
14-Oct	80	Measure PD response
14-Oct	80	Measure RC2 response
15-Oct	80	Measure beam uniformity with trap and PD response
15-Oct	81	Measure RC3 response w/ 7B1
16-Oct	81	Measure beam uniformity with trap and PD response
16-Oct	82	Measure beam uniformity with trap
16-Oct	82	Measure filter transmission at 532 w/ PD
16-Oct	82	Measure RC3 response w/ 7B1
17-Oct	82	Measure beam uniformity with trap and PD Response
18-Oct	83	Setup Ti-Sapphire for spectral measurements
18-Oct	83	Filter Response measurements
21-Oct	87	Window Transmission measurements

Table 2a. NISTAR photodiode spectral response data filenames and wavelength ranges for the system-level filter transmittance measurements. The filenames in the second column contain the timestamps data files and have the format YYMMHHDDmm, where YY = year, MM = month, DD = day of month, HH = hour of day, and mm = minutes into hour. To identify the filters, the NISTAR filter wheel (FW) motor positions in stepper motor counts are used as column headings, such as FW3, FW202, etc. FW3 brings an open (no-filter) position in the filter wheel in front of the NISTAR PD, whereas the others bring either Band B or Band C filters in front of the NISTAR PD, as indicated. Orange highlights indicate OPEN filter positions, blue indicates Band C measurements and green indicates Band B measurements. The wavelength range indicates the nominal start stop positions of the Ti:Sapphire scan.

Notebook Page	Filename	Wavelength Start	Wavelength Stop	FW Position	Comments
83	RC1310182139.txt	700	735	FW3	OPEN
83	RC1310182208.txt	700	735	FW202	Band C
83	RC1310182217.txt	700	735	FW502	Band C
83	RC1310182224.txt	700	735	FW902	Band C
83	RC1310182224.txt	700	735	FW302	Band B
83	RC1310182239.txt	700	735	FW802	Band B
84	RC1310182243.txt	700	735	FW1101	Band B
84	RC1310182337.txt	720	750	FW3	OPEN
84	RC1310182341.txt	720	750	FW202	Band C
84	RC1310182345.txt	720	750	FW502	Band C
84	RC1310182355.txt	720	750	FW902	Band C
84	RC1310182359.txt	720	750	FW302	Band B
84	RC1310190002.txt	720	750	FW802	Band B
84	RC1310190005.txt	720	750	FW1101	Band B

Table 2b. This table contains the correction coefficients derived from the fitting the 2013 system level data to the 2010 system level data for each filter, along with their estimated uncertainty. As mentioned in the analysis section above, these numbers serve to scale the 2010 results, which were more highly spectrally sampled and of a broader spectral range, to a corrected value. Blue highlights the Band C filters and green highlights the Band B filters.

Filter Name	Correction Coefficient	Uncertainty (%) k=1
1C1	1.047	0.1
5C2	1.050	0.1
8C3	1.034	0.1
7B1	1.019	0.1
2B3	1.043	0.1
11B2	1.024	0.1

Table 2c. NISTAR photodiode and trap detector spectral response measurement data filenames, and corresponding spectral ranges. The filenames in the second column follow the same timestamp file convention described in Table 2a. Beige highlights NISTAR photodiode response files and yellow highlights trap detector response files.

Notebook Page	Filename	Wavelength Start	Wavelength Stop	Detector	Comments
87	RC1310221701.txt	696	740	PD	No Window
87	RC1310221716.txt	696	740	PD	PD Window
87	RC1310221725.txt	696	740	Trap	

Table 3. NISTAR response measurements during 2013 system-level calibration, along with the corresponding trap detector measurements, all at a wavelength of 532 nm. The filenames in the second column follow the same timestamp file convention described in Table 2a. The RC shutter cycle runs are highlighted in blue and the trap measurements are highlighted in green. The first trap measurement follows a different filename convention due to the nature of the measurement performed. In this convention the last 6 numbers in the filename represent YYMMDD.

Notebook Page	Filename	Measurement	Number of Shutter Cycles	start:stop index	Trap Value	Trap Error	RC Value	RC Error
76	ExtTrapXscanN03 131009.txt ExtTrapYscanN01 131009.txt	**Trap**			-2.6906	2.809E-04		
76	RC1310100003.txt	**RC1**	53	322:32122			1.579E-06	2.507E-09
76	RC1310101115.txt	**RC2**	44	1717:28117			1.592E-06	2.891E-09
77	RC1310102017.txt	**Trap**			-2.6835	2.438E-05		
77	RC1310102111.txt	**RC3**	73	435:44235			1.564E-06	2.741E-09
77	RC1310111122.txt	**Trap**			-2.6879	2.401E-05		
77	RC1310111635.txt	**RC1 repeat**	110	7:66007			1.575E-06	1.775E-09
78	RC1310121202.txt	**Trap**			-2.6844	2.388E-05		
78	RC1310121245.txt	**Trap**			-2.6855	2.523E-05		
78	RC1310121422.txt	**RC2 repeat**	124	77:74477			1.586E-06	1.971E-09
78	RC1310131300.txt	**Trap**			-2.6859	2.699E-05		
79	RC1310131402.txt	**RC3 repeat**	115	81:69081			1.564E-06	2.189E-09
79	RC1310141020.txt	**Trap**			-2.6836	2.221E-05		
80	RC1310141538.txt	**RC2 repeat 2**	117	7:70207			1.583E-06	2.026E-09
80	RC1310151207.txt	**Trap**			-2.6839	3.276E-05		

Table 4. Chamber window transmittance measurement results for the 2013 NISTAR calibration, at a wavelength of 532 nm. The filenames in the first column follow the same timestamp file convention described in Table 2a.

Filename (RCYYMMDDHHmm.txt)	Window Port	PD Window In (A)	dPD Window In (A)	PD Window Out (A)	dPD Window Out (A)	PD Shutter Closed (A)	τ_w	$d\tau_w$ (%)
RC1310222310.txt	PD	2.462E-07	6.095E-11	2.486E-07	9.925E-11	9.647E-11	0.99019	0.0470
RC1310222324.txt	RC1	2.457E-07	3.710E-11	2.486E-07	9.925E-11	9.647E-11	0.98818	0.0427
RC1310222317.txt	RC2	2.452E-07	3.622E-11	2.486E-07	9.925E-11	9.647E-11	0.98652	0.0426
RC1310222330.txt	RC3	2.480E-07	3.679E-11	2.486E-07	9.925E-11	9.647E-11	0.99767	0.0426

Table 5. Summary of the 2013 system-level absolute calibration results for the three NISTAR ACRs at a wavelength of 532 nm. Note the table is incomplete and results for the gain of the trap pre-amplifier and the trap responsivity are missing. These will be included in the full calibration report once the measurements have taken place at NIST.

Measurement			**RC1**		**RC1 repeat**	
Parameter Description	**Type of Uncertainty**	**Parameter (Units)**	**Value**	**Uncertainty (%)**	**Value**	**Uncertainty (%)**
Gain of Trap Pre-amplifier	B	G_T (V/A)				
Irradiance Responsivity of Trap	B	R_T (Amm2/W)				
Beam Non-Uniformity	A	B	1.0000	0.0104	1.0014	0.0156
Chamber Window Transmittance	A	t_w	0.9882	0.0427	0.9882	0.0427
Response of Trap	A	r_T (V)	-2.691		-2.6861	0.0013
Response of NISTAR	A	r'_N (W)	1.579E-06	0.1588	1.575E-06	0.1127
Area of NISTAR ACR Aperture	B	A_N (mm^2)	49.8558	0.0030	49.8558	0.0030
Responsivity Coefficient	**combined**	C_N (W/Vmm^2)	-1.191E-08	0.1648	-1.188E-08	0.1216
Irradiance Responsivity of NISTAR	**combined**	$\boldsymbol{R_N}$				

Measurement	**RC2**		**RC2 repeat**		**RC2 repeat 2**	
Parameter (Units)	**Value**	**Uncertainty (%)**	**Value**	**Uncertainty (%)**	**Value**	**Uncertainty (%)**
G_T (V/A)						
R_T (Amm2/W)						
B	1.0027	0.0209	0.9999	0.0162	1.0000	0.0184
t_w	0.9865	0.0426	0.9865	0.0426	0.9865	0.0426
r_T (V)	-2.6835	0.0009	-2.6857	0.0014	-2.6837	0.0015
r'_N (W)	1.592E-06	0.1816	1.586E-06	0.1243	1.583E-06	0.1279
A_N (mm^2)	49.9745	0.0030	49.9745	0.0030	49.9745	0.0030
C_N (W/Vmm^2)	-1.200E-08	0.1877	-1.198E-08	0.1324	-1.197E-08	0.1361
$\boldsymbol{R_N}$						

Measurement	**RC3**		**RC3 repeat**	
Parameter (Units)	**Value**	**Uncertainty (%)**	**Value**	**Uncertainty (%)**
G_T (V/A)				
R_T (Amm2/W)				
B	1.0003	0.0116	1.0006	0.0189
t_w	0.9977	0.0426	0.9977	0.0426
r_T (V)	-2.6879	0.0009	-2.6847	0.0013
r'_N (W)	1.564E-06	0.1752	1.564E-06	0.1400
A_N (mm^2)	50.0166	0.0030	50.0166	0.0030
C_N (W/Vmm^2)	-1.166E-08	0.1807	-1.167E-08	0.1476
$\boldsymbol{R_N}$				

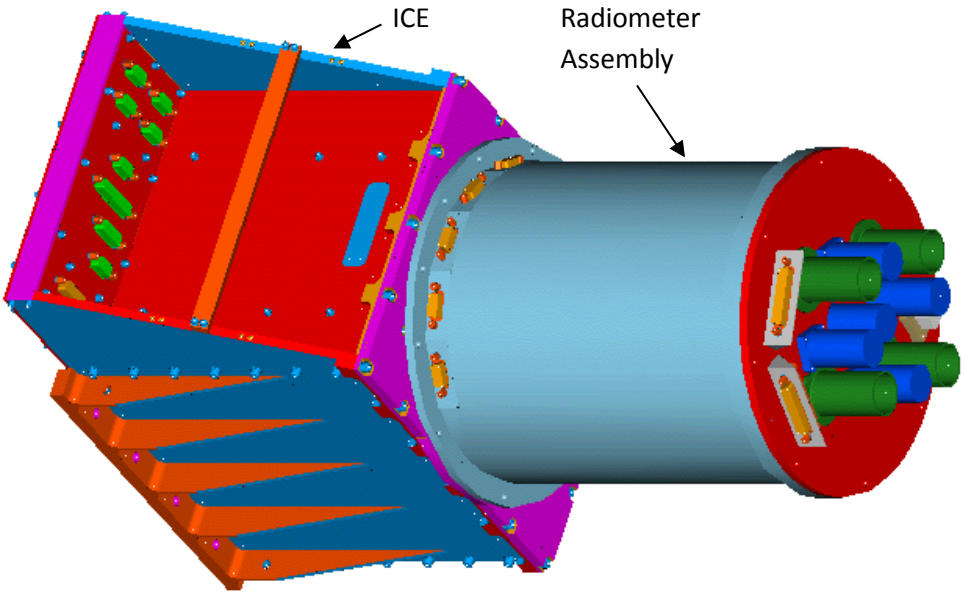

a)

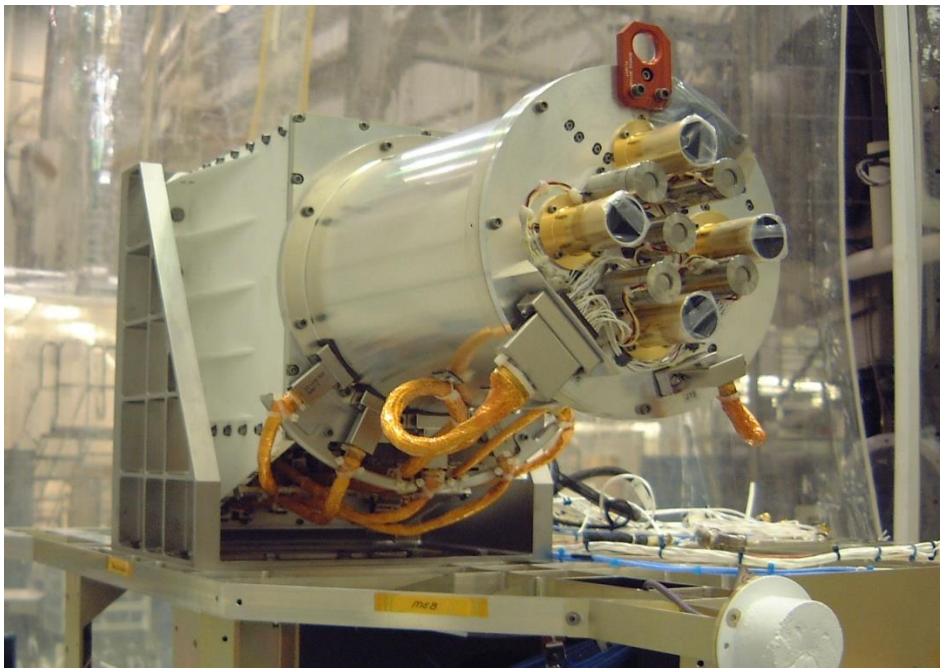

b)

Figure 1. NISTAR Radiometer Assembly and Interface Control Electronics (ICE). a) Drawing from solid model, b) Picture taken during fit check to DSCOVR spacecraft at NASA GSFC.

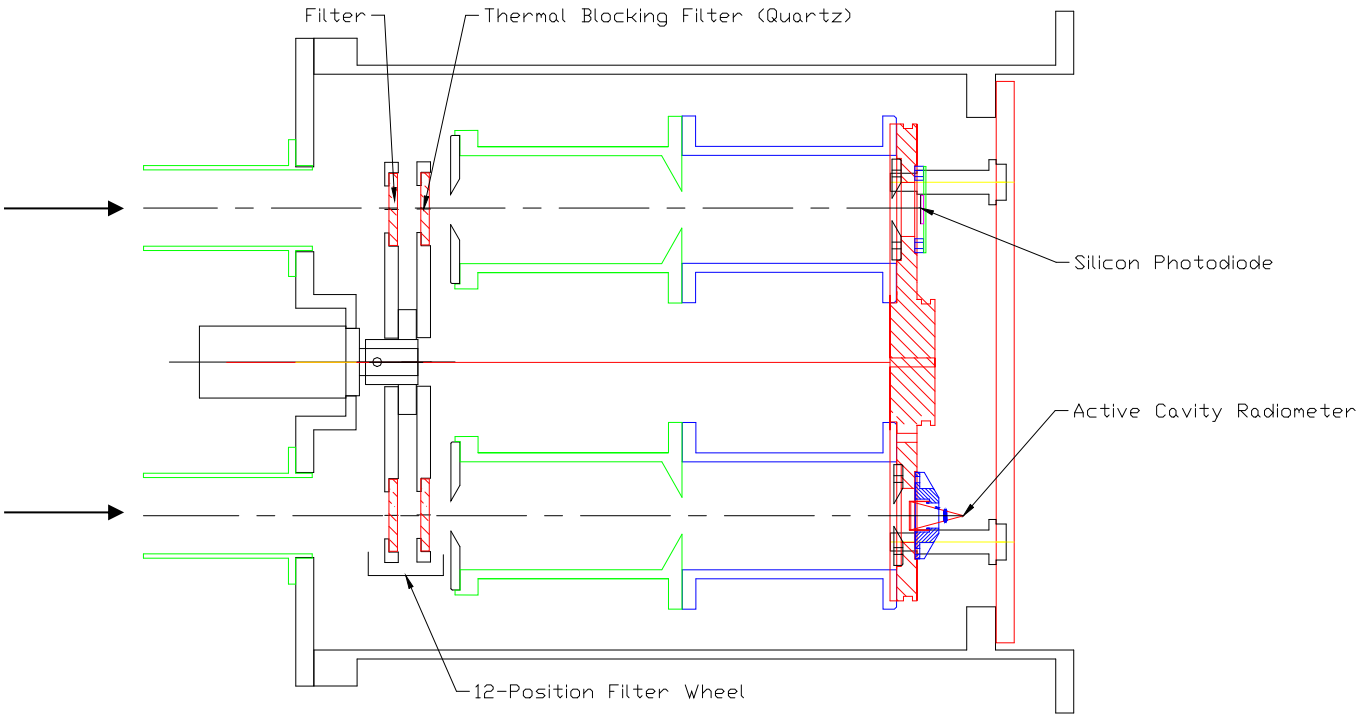

Figure 2. Cross-section of the NISTAR instrument radiometer assembly. The arrows coming from the left indicate the direction of the light to be measured. Note that the direction of the bevels of the primary apertures (the ones directly in front of the detectors) were flipped relative to that shown in this older drawing, as part of the 2002 instrument refurbishment. The motor for the filter wheel is shown, but the internal NISTAR shutters and the corresponding 4 shutter motors do not appear in this cross-section in the open shutter position.

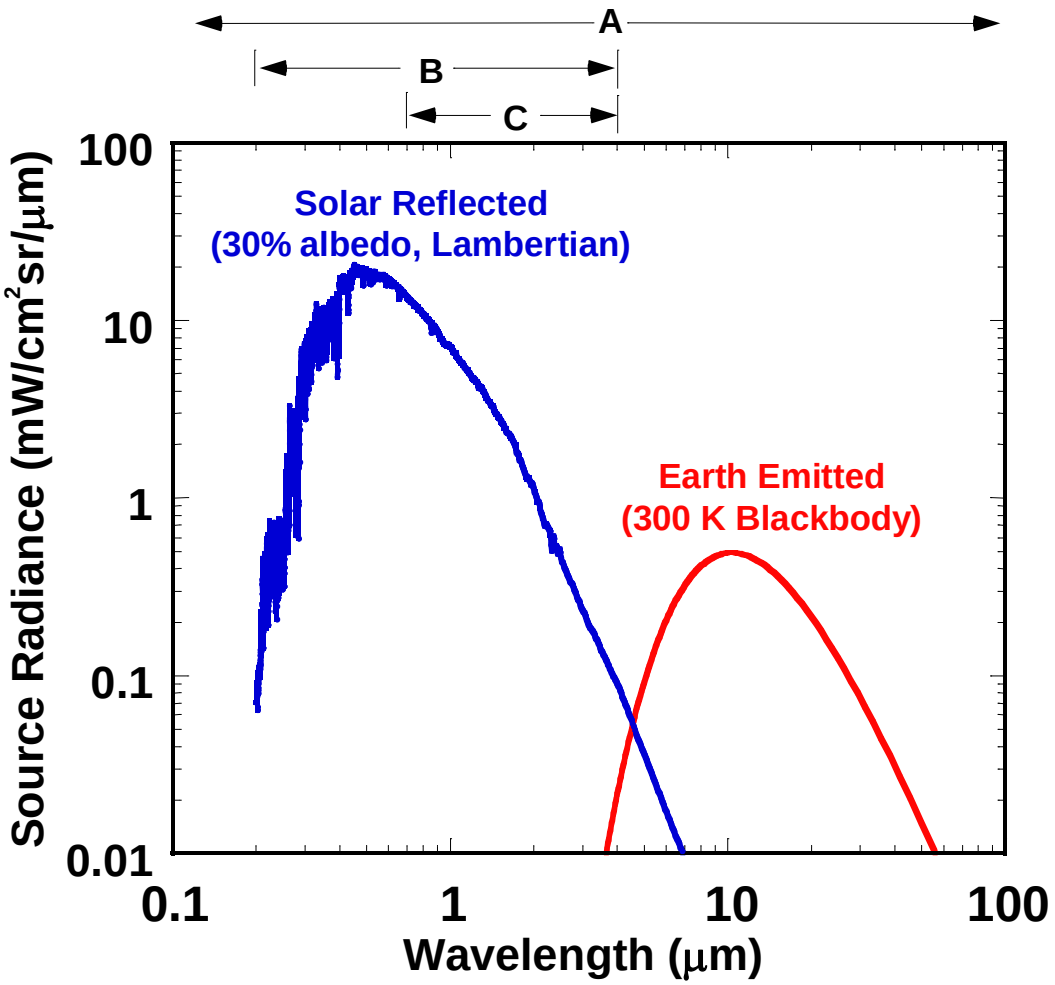

Figure 3. The range of the three NISTAR spectral bands, A, B, and C, shown in comparison to a very rough approximation of the expected radiance reflected and emitted from Earth towards the L-1 point.

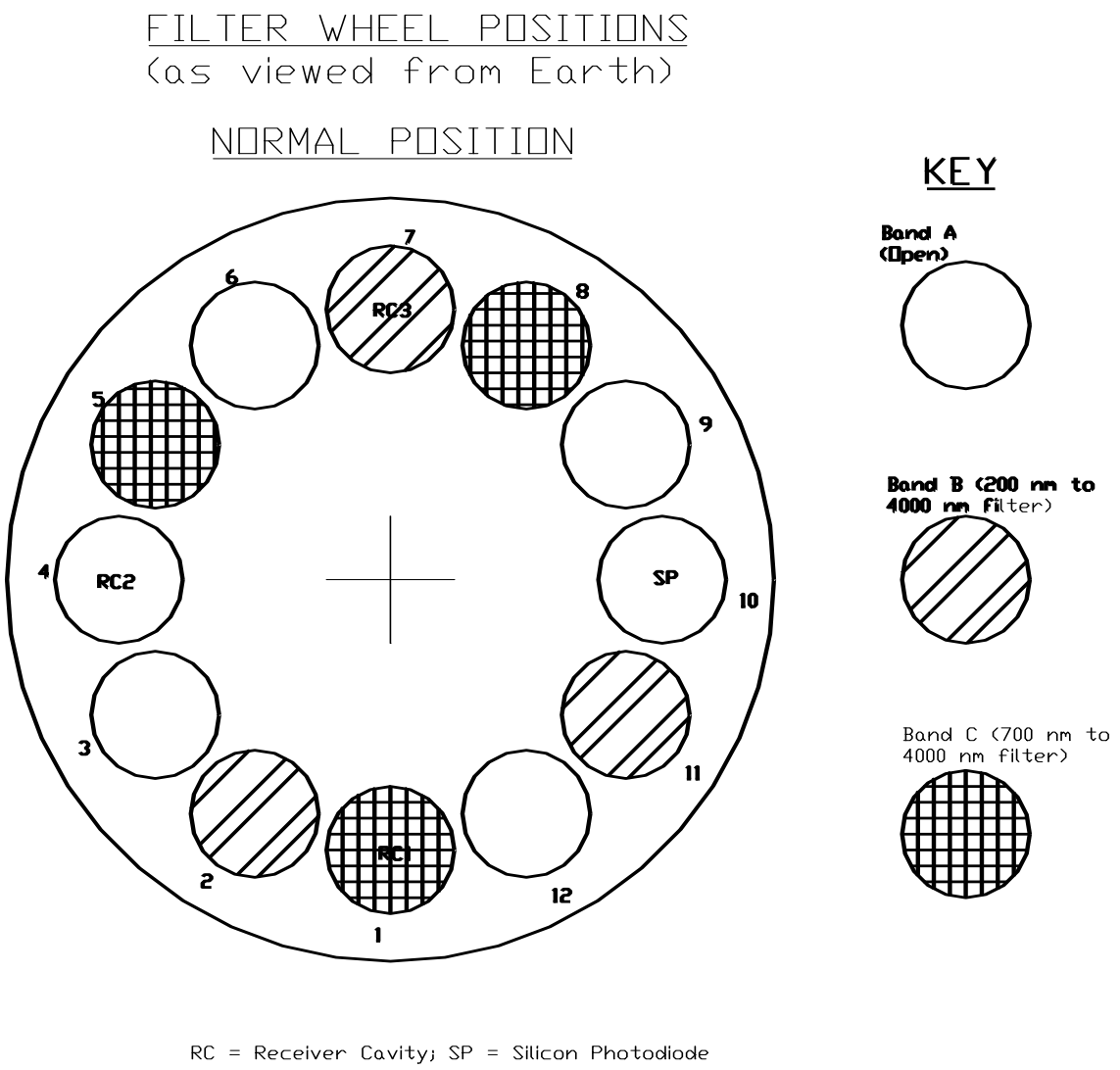

Figure 4. Layout of the filters on the NISTAR 12-position filter wheel. The filter wheel can rotate about its center, while the three receiver cavities (RC1, RC2, and RC3) and the silicon photodiode (SP) remain fixed, such that any filter can be placed in front of any of these four detectors. In the normal position shown, RC1 measures Band C, RC 2 measures Band A, and RC3 measures Band B.

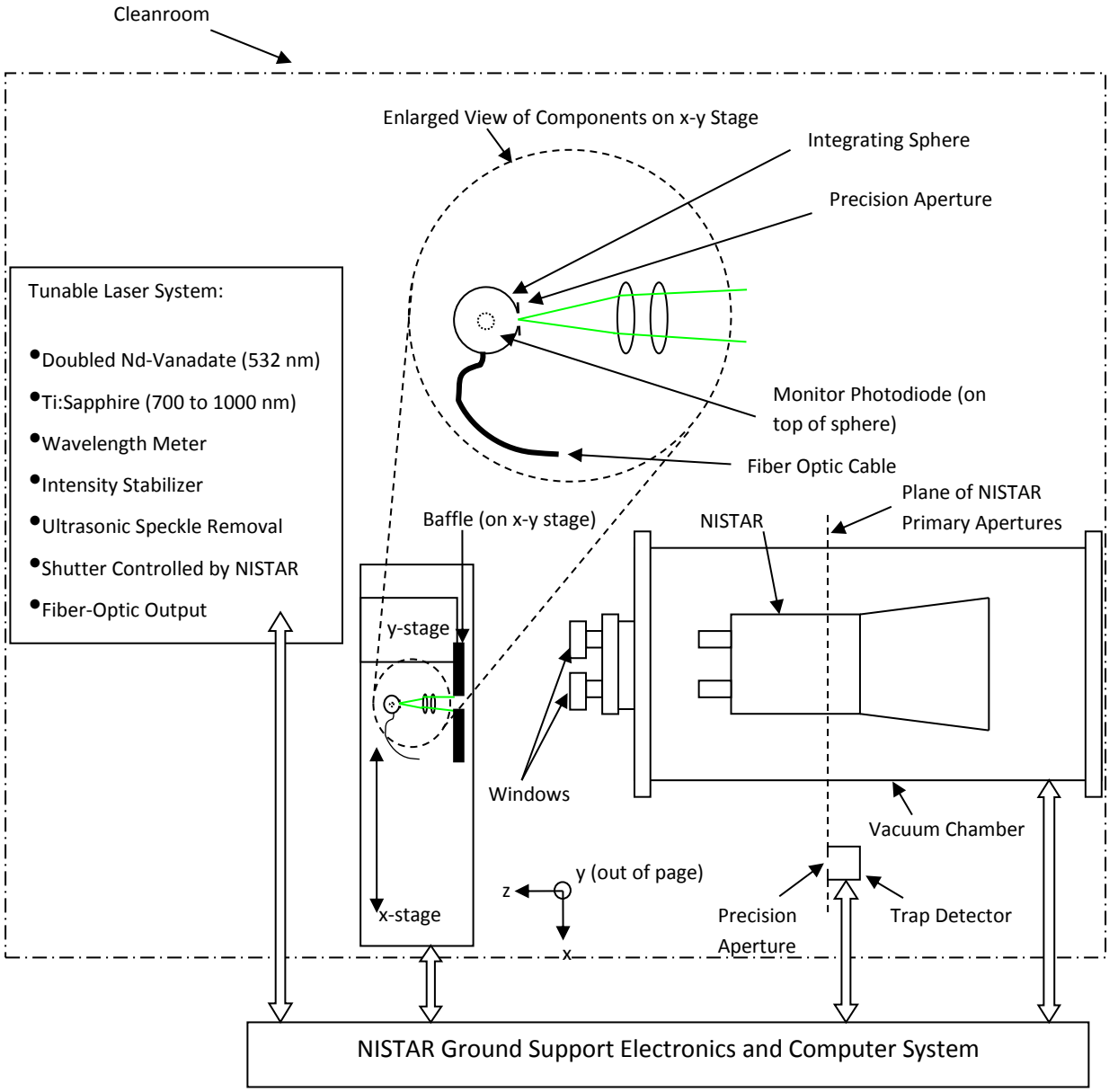

Figure 5. Layout of the system used for the 2013 system-level calibration of NISTAR at L-1 Standards and Technology. The chamber, x-y stage, and laser system were in a darkened clean room, and the NISTAR ground support electronics systems were outside of the clean room. A fiber-optic cable coupled the light from the laser system to the integrating sphere shown here. The green rays represent the light beam sent alternately to NISTAR or to the trap detector. This drawing is not to scale.

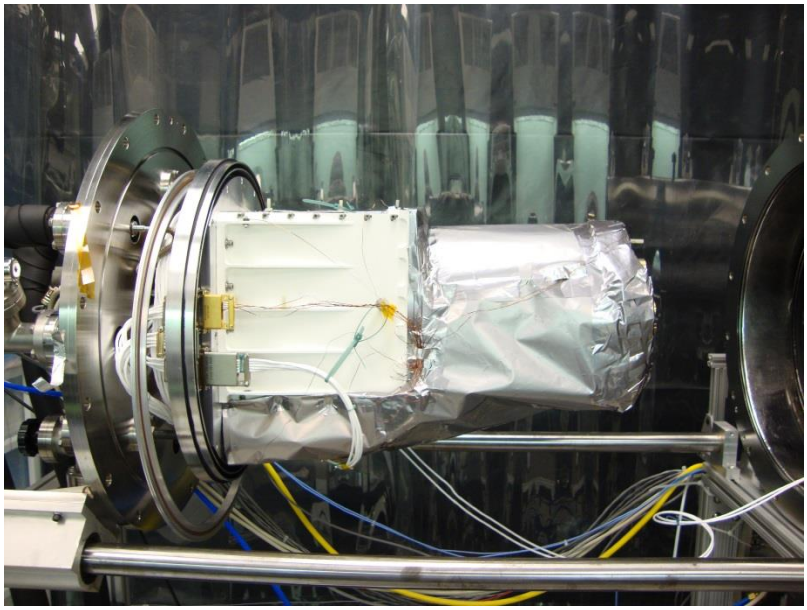

Figure 6a. Picture of the NISTAR instrument after it was prepared and mounted on the chamber.

Figure 6b. Picture of the laser and accessories comprising the uniform source system at L-1 Standards and Technology, Inc.

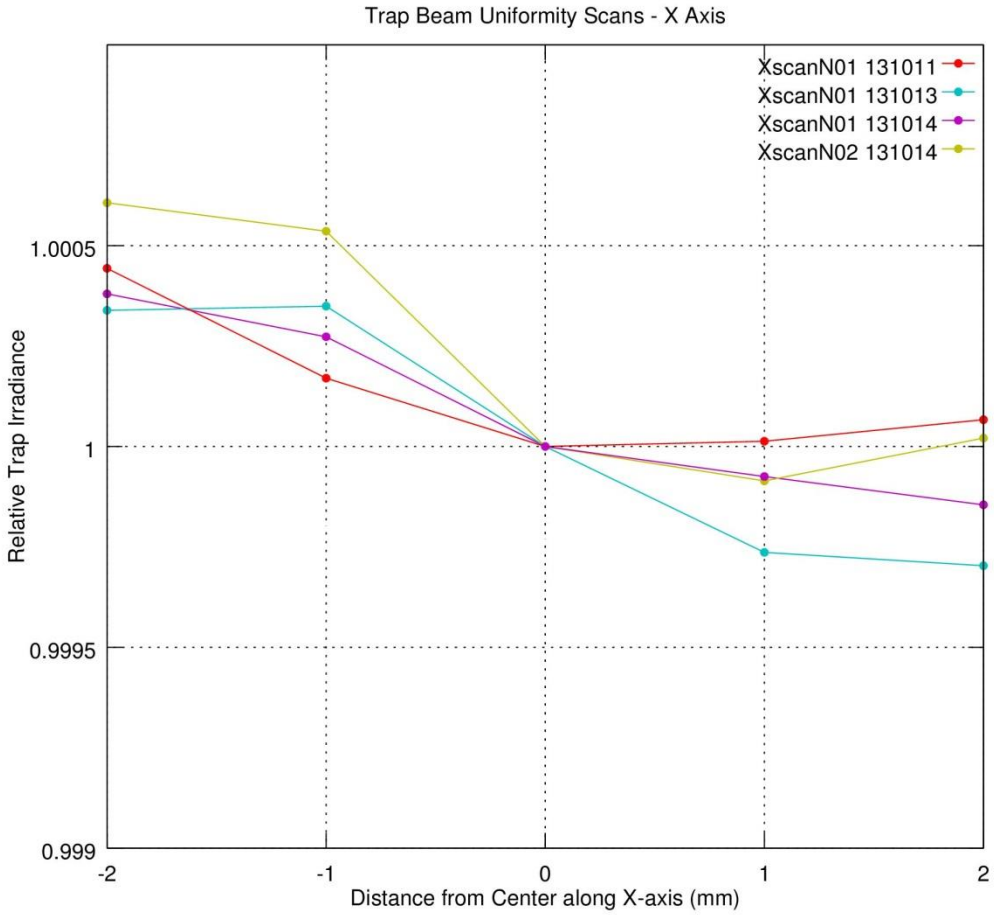

Figure 7. Results from scanning the collimated light beam across the trap detector in the x-direction. The x-domain represented here shows the effective aperture as seen by the NISTAR instruments. The distances reported in this plot are relative to the center stage position for the trap detector. Different curves indicate scans from various days.

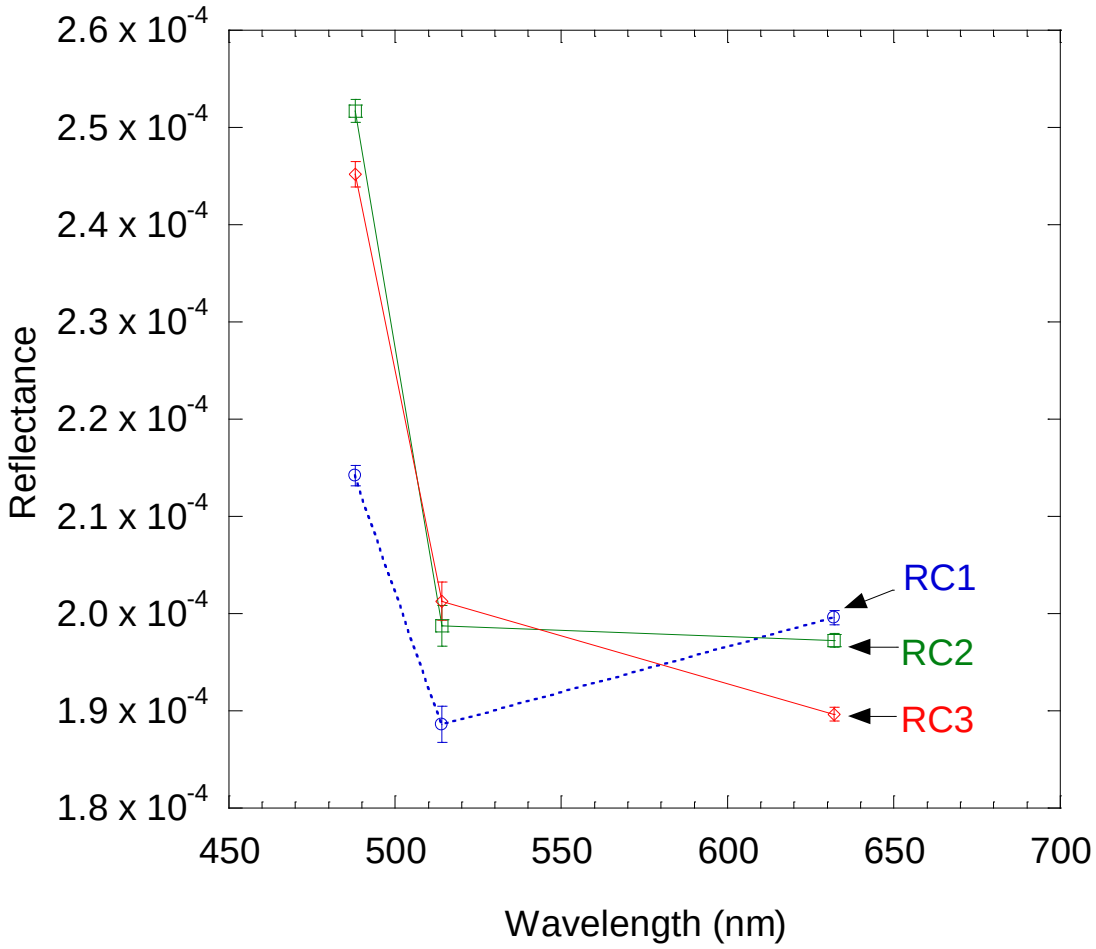

Figure 8. Reflectance of the NISTAR flight receiver cavities, RC1, RC2, and RC3, measured at NIST in January 2003 just prior to installation in the NISTAR instrument. The measurements were made using a Spectralon integrating sphere at three laser wavelengths: 488 nm, 514 nm, and 633 nm. The empty sphere sample port was used as a dark reference, and a pressed PTFE pellet at the sample port, replacing the cavity under test, was used as the white reference standard. The error bars indicate the k=1 uncertainty that resulted from measurement noise. The lines are guides for the eye.

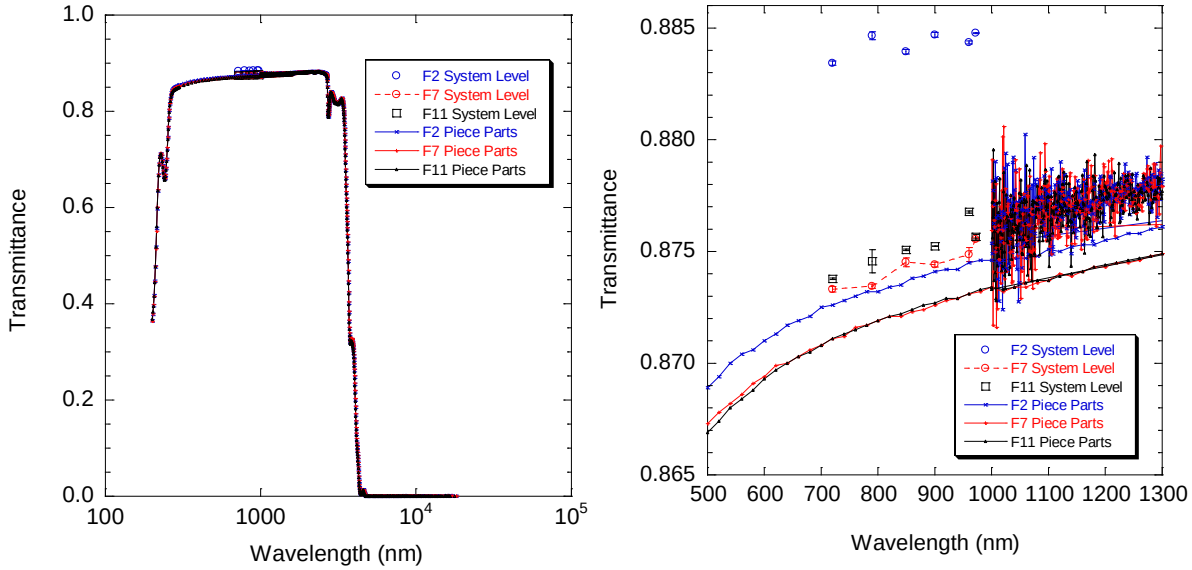

Figure 9. Transmittance of all Band B filters as measured from the piece parts and from the 2001 system-level SIRCUS calibration: a) Full range, b) Expanded view of VNIR range.

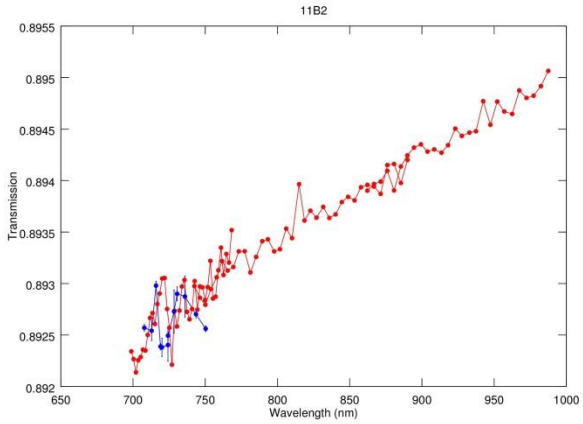

a)

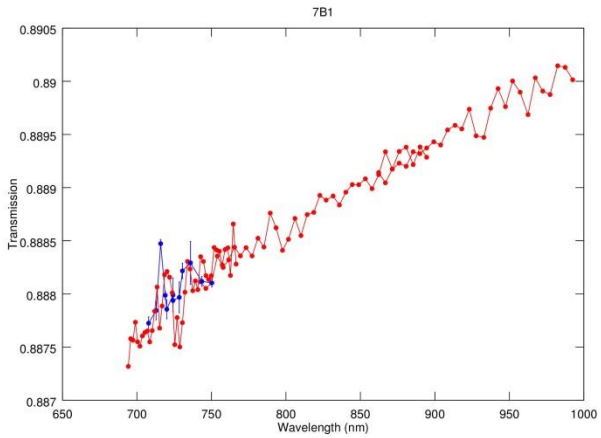

b)

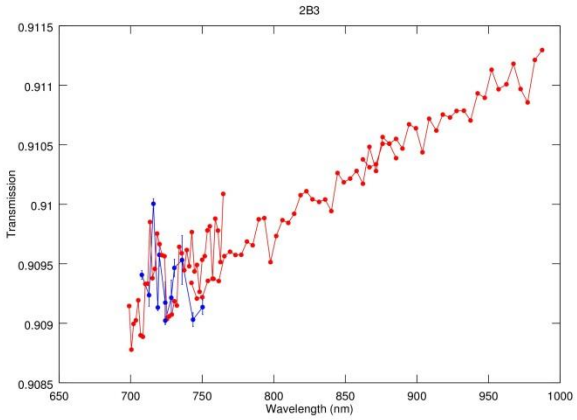

c)

Figure 10. Transmittance of Band B filters as measured in 2013 (blue) with the corrected 2010 system-level measurements superimposed (red). The correction coefficients were pulled from Table 2b.

a) F11 b) F7 c) F2

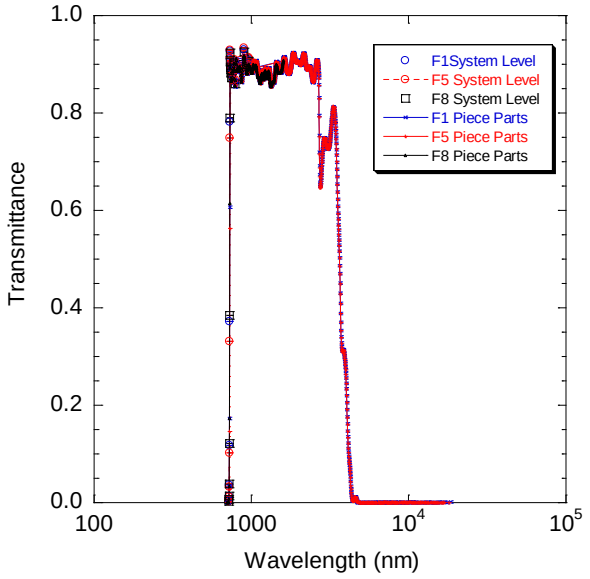

a)

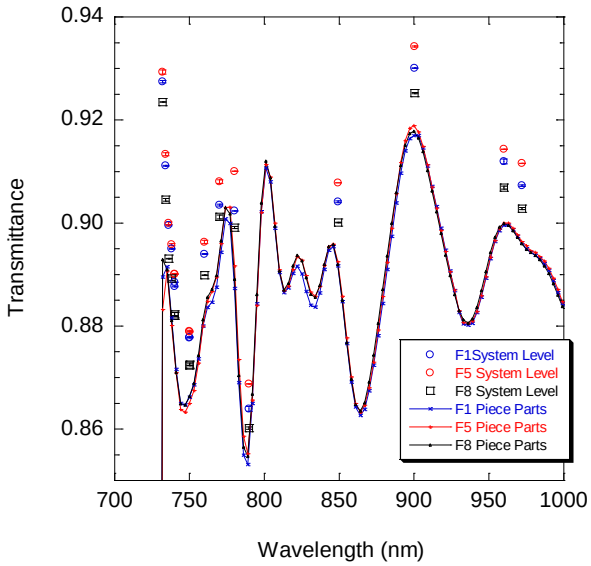

b)

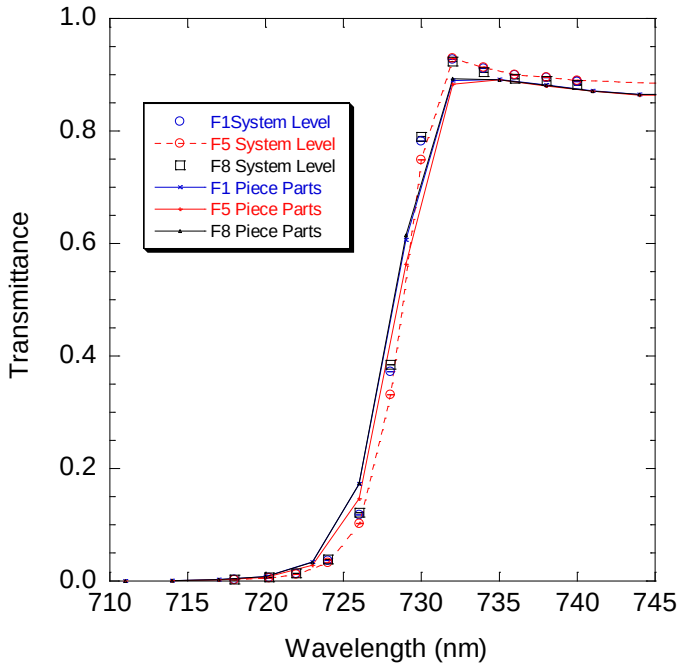

c)

Figure 11. Transmittance of all Band C filters, as measured from the piece parts and from the 2001 system-level SIRCUS calibration: a) Full range, b) Expanded view of VNIR range, c) Expanded view of the transition region.

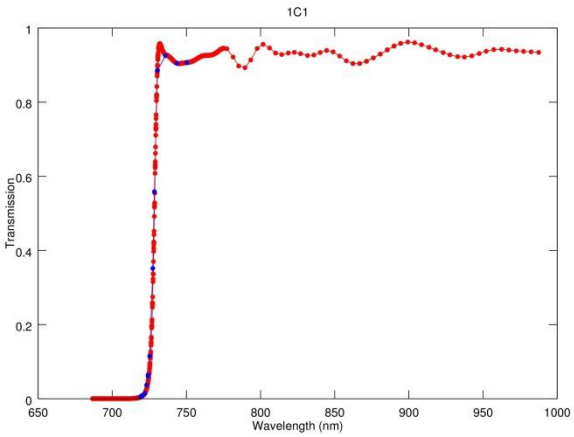

a)

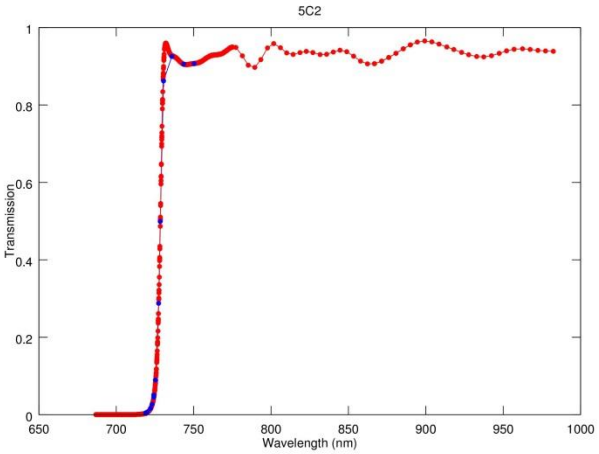

b)

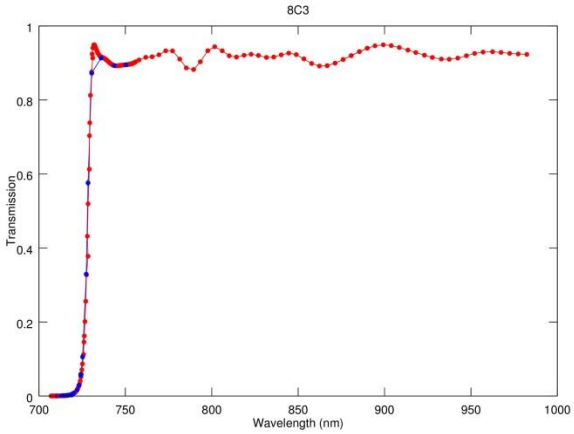

c)

Figure 12. Transmittance of Band C filters as measured in 2013 (blue) with the corrected 2010 system-level measurements superimposed (red). The correction coefficients were pulled from Table 2b.

a) F1 b) F5 c) F8

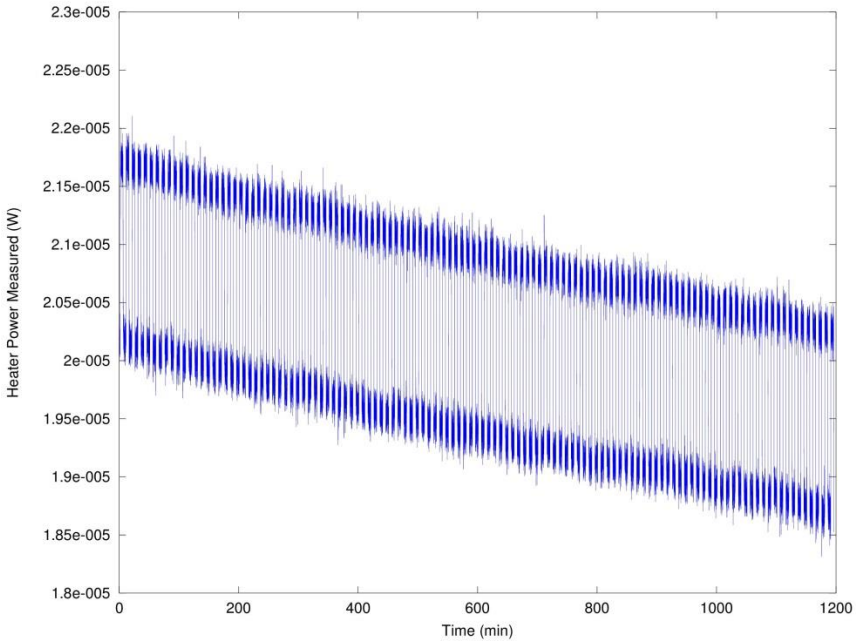

a)

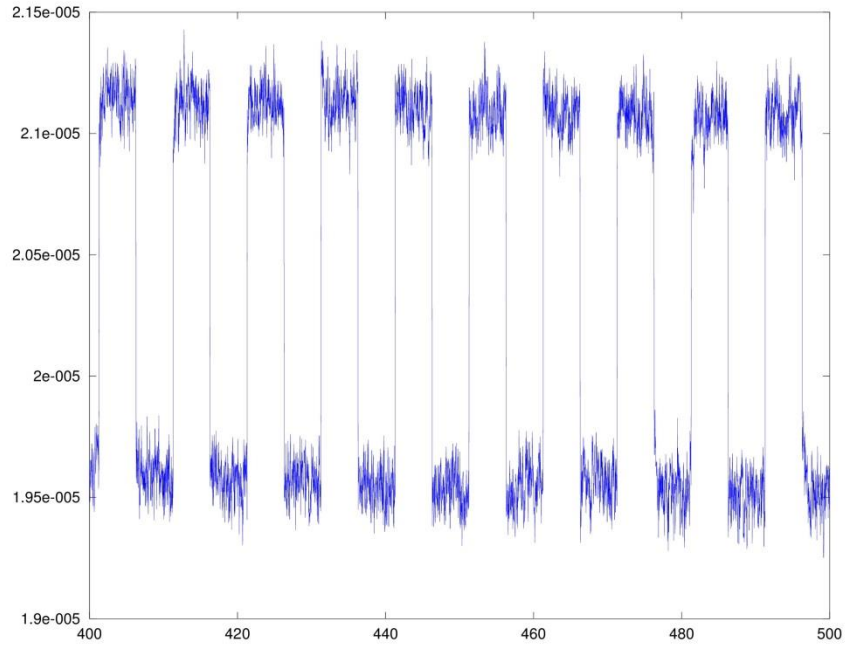

b)

Figure 13. NISTAR response measured by a typical receiver cavity (RC3) during absolute calibration: a) Full scale, b) Expanded scale between 400 min. and 500 min.

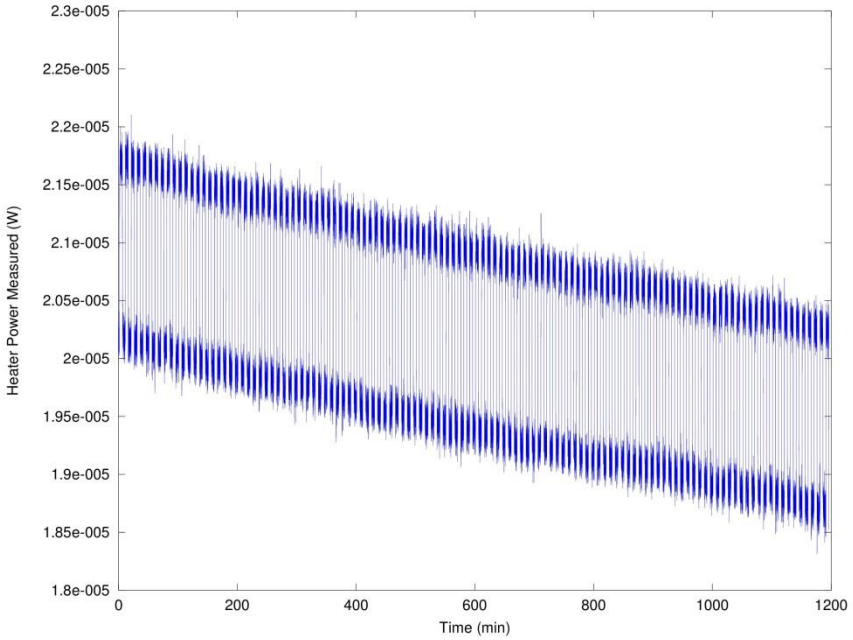

a)

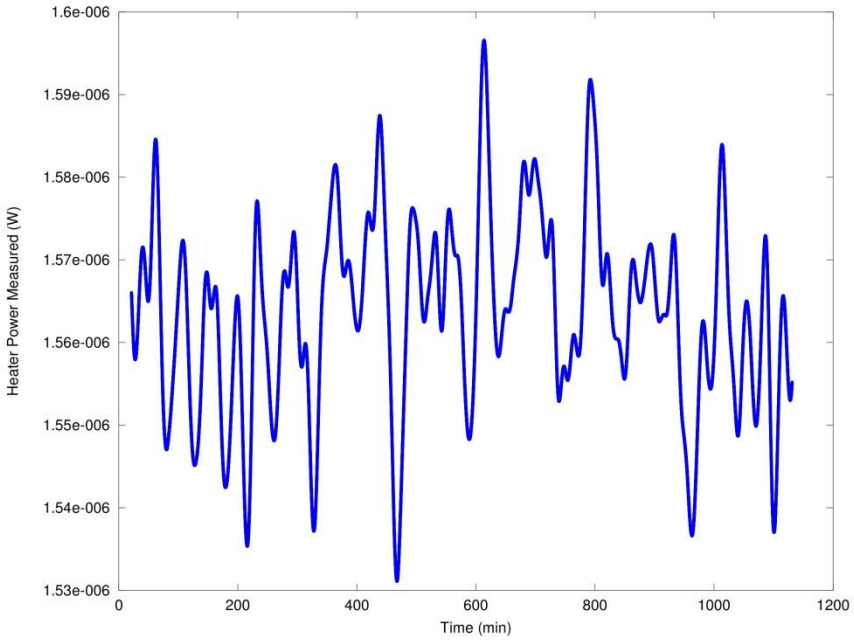

b)

Figure 14. Example results, for RC3 response during the 2013 calibration, from the analysis by the phase-sensitive detection algorithm: a) input, b) output.

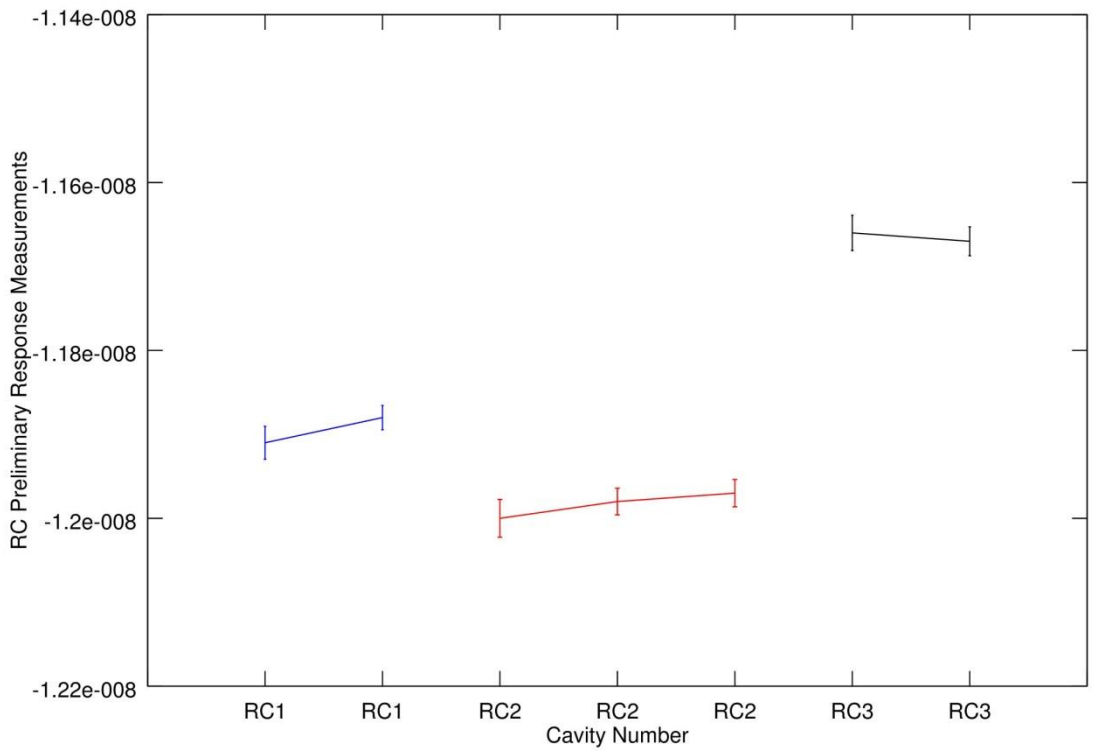

`

Figure 15. Summary results from the 2013 NISTAR preliminary system-level calibration as shown in Table 5. These preliminary measurements indicated the responsivity of the cavities without the calibrated scale factors from the trap irradiance responsivity or the gain of the trap pre-amplifier. The error bars indicate the combined standard uncertainty of the comparison as discussed in the text. Different points for the same RC indicated repeated measurements on separate days.

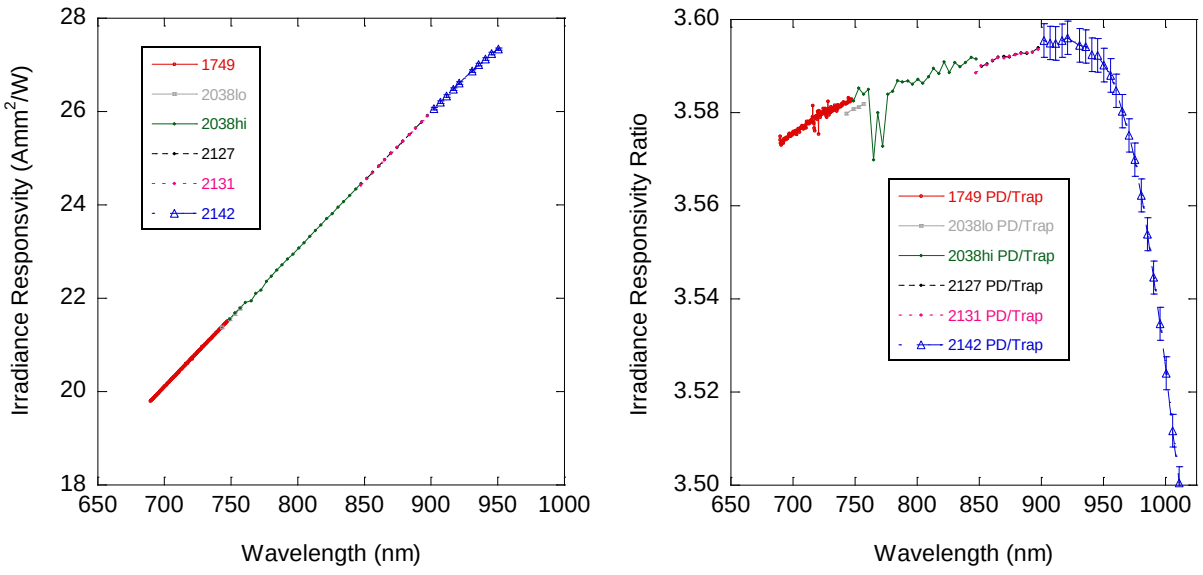

a) b)

Figure 16. 2010 measurements of the NISTAR PD responsivity. These results will be fit to the 2013 calibration results included in the upcoming full calibration report.

a) System-level absolute spectral irradiance responsivity of the NISTAR Photodiode in Band A.

b) Ratio of the NISTAR Photodiode Band A irradiance responsivity to that of the trap detector used in 2010. The different colored ranges were measured during separate scans on the same day (16 August 2010), with PD scan time-of-day start time in hours (H) and minutes (M) as indicated in the legend in the format (HH:MM). PD data were measured only at the wavelengths indicated by a symbol, and the trap data were interpolated to those wavelengths. The lines are a guide for the eye. The error bars, plotted only on the last segment for clarity, illustrate how the estimated 0.1 % (k=1) uncertainty level compares with the repeatability of segments in overlapping spectral regions.